Computational Materials Science 191 (2021) 110306

Contents lists available at ScienceDirect

Computational Materials Science

journal homepage: www.elsevier.com/locate/commatsci

Identifying key parameters for predicting materials with low defect generation efficiency by machine learning

Dongyuan Ni [a,b], Wei Wu [b], Yaguang Guo [a,b], Sheng Gong [b], Qian Wang [a,b,*]

[a] Center for Applied Physics and Technology, HEDPS, College of Engineering, Peking University, Beijing 100871, China
[b] BKL-MEMD, School of Materials Science and Engineering, Peking University, Beijing 100871, China

ARTICLE INFO

Keywords:
Low defect generation efficiency
Machine learning

ABSTRACT

The primary radiation damage is an important part of the radiation process, which is of current interest as the rapid development of nuclear reactors and space instrumentation. In this study, using machine learning, we have demonstrated that atomic mass difference, Poisson's ratio, mean atomic mass, and mass density have significant influence on the defect generation efficiency of a material during the primary damage step. Furthermore, we construct a new dataset by using these important features and obtain a well-trained neural network for predicting new materials with low efficiency of defect generation. In our study, the target of the dataset for training the predictor is constructed using the results from molecular dynamics simulations. This work provides the guiding information for designing materials with low efficiency of defect generation.

1. Introduction

It has been an important task to seek for materials that are robust against irradiation in some devices such as fusion and fission reactors [1], space stations [2], and nuclear robotics [3], where high irradiation dose can induce swelling, hardening, creep, and amorphization in materials [4]. So far, some studies have been done for the physical phenomena of materials under irradiation using molecular dynamics method, i.e. defects formation [4,5], impacts on elastically stressed crystallites [6], and edge dislocations [7], etc. The ideal radiation-tolerant materials should meet two basic requirements: (1) Few defects are generated under irradiation; (2) Defects can be rapidly annihilated or absorbed during annealing [8]. It is important to note that the dynamics of defects is closely related to the following physical quantities: (a) Configurational information. High configurational entropy can largely suppress the formation of dislocation loops, then enhance the phase stability of materials [9,10]. For instance, tungsten (W)-based alloys composed with Ta, Cr, V exhibit outstanding radiation tolerance and thermal stability compared with low entropy alloys [11]; (b) Chemical bond. Low activation energy barriers will facilitate the propagation and diffusion of point defects to promote recrystallization [12,13]; (c) Mechanical properties. Amorphization can be induced by the ductile-to-brittle transition, which is related to Pugh criterion, Cauchy pressure, and Poisson's ratio [14], etc.; (d) Irradiation intensity. High-energy irradiation has large stopping power, which can generate heat and lead to amorphization [15–17]. Previous studies only focus on two or three materials [8,18–21]. As the number of materials increases, it is better to use numerical analysis techniques and data mining [22] to obtain statistical results.

Machine learning (ML) has been widely used in materials science for guiding chemical synthesis, predicting properties of materials, and constructing molecular dynamics potentials [22–24], etc. The core of ML is building a mapping between the target and some relevant parameters. Once the mapping is built, it can predict the target and establish a numerical interpretation of the dataset, where the dominated features make more contributions to training ML models, and the underlying physics can be deduced by the numerical importance of features, in other words, feature importance. Pilania and his co-authors have studied the connection between the amorphization of irradiated pyrochlores and some fundamental factors [25], demonstrating the capability of ML method in discovering the relationship between intrinsic features and defect generation efficiency (DGE) of materials. The primary damage is a crucial part of the whole radiation process, which can help us understand the defect generation [26,27]. Furthermore, the defect generation of primary damage is closely related to the properties of pristine materials rather than damaged materials, then is

* Corresponding author at: Center for Applied Physics and Technology, HEDPS, College of Engineering, School of Materials Science and Engineering, Peking University, Beijing 100871, China.
E-mail address: qianwang2@pku.edu.cn (Q. Wang).

https://doi.org/10.1016/j.commatsci.2021.110306
Received 13 September 2020; Received in revised form 9 January 2021; Accepted 11 January 2021
Available online 4 February 2021

suitable for the feature data acquisition before training ML models.

In this work, we have trained three ML models (i.e. kernel ridge regression (KRR) [25,28], decision tree [29,30], and neural network [24]) using our dataset constructed by a series of elemental materials and binary compounds, and all of three models give acceptable results. Moreover, the decision tree can provide the feature importance to point out significant features. Our results show that atomic mass difference, Poisson's ratio, mean atomic mass, and mass density are the important features of materials for defect generation in primary damage. To reduce the requirements that the predicted low DGE materials should meet, we only use these four important features combined with two environmental features to build a new dataset, named dataset-6. The dataset-6 is used to train ML models and the well-trained model can predict new low DGE materials.

2. Computational methods

Molecular dynamics method [31–33] is used to simulate ballistic cascade. To avoid the error from different symmetries, all of the selected materials possess $Fm\bar{3}m$ symmetry. In total, 18 single-element materials and 21 binary compounds are collected from Materials Project [34]. LAMMPS [35] code is used to carry out the simulations for each of them with a supercell of $30 \times 30 \times 30$. The embedded-atom method (EAM) [36], angular-dependent potential (ADP) [37], and Tersoff potential [38,39] are used for the interatomic interactions. The primary knocked-on atom (PKA) at the centroid of the cubic supercell with initial kinetic energy is introduced [40], and the PKA interacts with its neighbors to simulate collision cascade. The total simulation time is 1 ps with a time step of 0.01 fs, which is used for the whole primary damage process [41]. The systems are restricted by the NVE ensemble to keep the process adiabatic [42]. The numbers of vacancies and interstitials are counted by using Wigner-Seitz defect analysis method *via* Open Visualization Tool (OVITO) [43]. To study the influence of different kinetic energies of PKA and directions of PKA's velocity, the energies of 2, 5, 8, and 10 keV, and the directions of [1 0 0], [1 1 0], and [1 1 1] are examined, and thus a dataset containing 444 samples is generated. KRR, decision tree, and neural network are employed as implemented in Scikit-learn (sklearn) [44] and PyTorch [45] packages.

3. Results and discussion

3.1. Constructing dataset

We first examine whether the supercell size of $30 \times 30 \times 30$ is adequate for simulating the ballistic cascade process. In brief, all samples are inspected and eligible. Taking the damage pattern of $AlNi_3$ shown in Fig. 1 as an example. One can see that the defects commonly distribute around the center of the cubic box, which means the irradiation process is hardly affected by the periodicity of crystals, implying the size of supercell is large enough for the study of irradiation.

Based on previous studies [46–49], we choose fourteen features and classify them in four groups, namely, (1) mean atomic radius, mean atomic mass, atomic mass difference, mass density, (2) formation energy, mean period, mean group, number of valence electrons, (3) shear modulus, bulk modulus, elastic anisotropy, Poisson's ratio, (4) kinetic energy of PKA, and direction of PKA's velocity to cover configurational information, chemical bond, mechanical properties, and irradiation intensity as mentioned in the introduction part. While for the target, we choose the defect ratio after cascade to represent the amorphization and the damage of a material after primary damage, and is calculated by dividing the number of defects by the total number of atoms. Fig. 2 shows the elements of the selected single-element materials and binary compounds in the dataset. Most of them are widely used in the area of radiation-tolerant materials, illustrating that the dataset is adapted for the study of seeking low DGE materials.

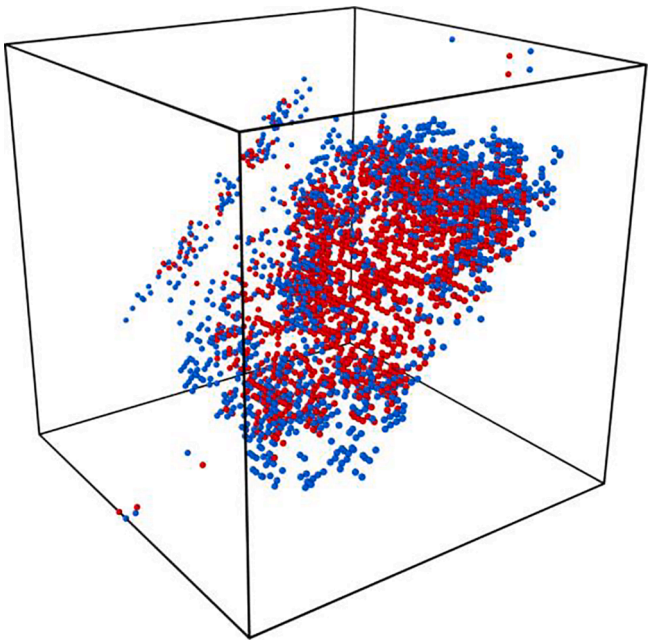

Fig. 1. Point defects distribution in the $AlNi_3$ supercell after 1 ps under the kinetic energy of PKA of 10 keV. The direction of PKA's velocity is along the [1 0 0]. The red and blue spheres represent the vacancies and interstitials generated by the ballistic cascade, respectively.

3.2. Training ML models

We implement three ML models, i.e. kernel ridge regression (KRR), decision tree, and neural network on our dataset. To measure the accuracy of the models, the normalized root mean squared error (NRMSE) [50], Pearson correlation coefficient (r) [51] between the targets and predicted values are calculated. The expression of NRMSE:

$$\mathrm{NRMSE} = \frac{1}{y_{max} - y_{min}} \sqrt{\mathrm{E}((y - \hat{y})^2)} \tag{1}$$

for r:

$$\frac{r = \sum (y - \bar{y})(\hat{y} - \bar{\hat{y}})}{\sqrt{\sum (y - \bar{y})^2 \sum (\hat{y} - \bar{\hat{y}})^2}} \tag{2}$$

where y and $\hat{y}$ *represent* the targets of the dataset and the predictions of the ML models, respectively. The NRMSE reflects the relative error between the targets and predictions. The r gives the degree of linear dependence as shown in Eq. (2). The learning curves of three ML models are plotted in Fig. 3. Moreover, the results of three ML models in Fig. 3 are averaged over 100 independent trials. For NRMSE, the values decrease with increasing data of the training set. As for r, the values increase with increasing of the training set. Both of them show better predicting ability of ML models as the expansion of the training set. The 90%-training-set results are the best and acceptable compared with other related works [28,52,53].

Among all of the ML models, the decision tree can not only do the prediction, but also provide the importance of each feature according to the optimization process [54]. The feature importance of the dataset is shown in Fig. 4(a), where the dominant features for defect generation are identified to be atomic mass difference (23.6%), kinetic energy of PKA (21.4%), Poisson's ratio (15.0%), mean atomic mass (11.3%), and mass density (9.1%). They can be classified into two groups, which are named the environmental feature and intrinsic features of materials. For the environmental feature, the kinetic energy of PKA could lead to various amorphization and channeling effects especially in high energy cases with strong penetration to affect deeper regions [55]. Thus, it has

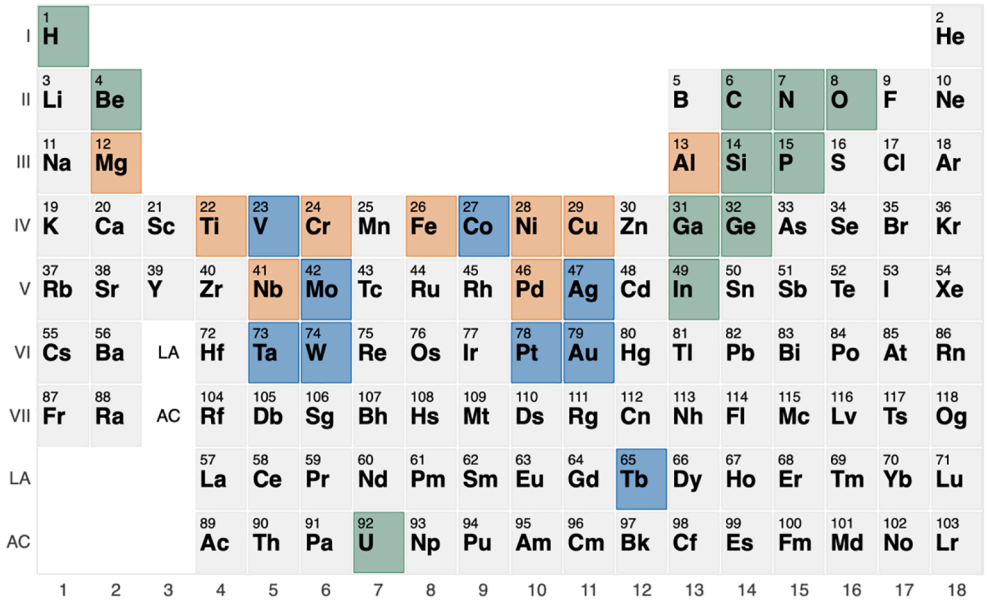

Fig. 2. Elements with the shadows in the periodic table for our studied materials. The blue, green, and orange shadows represent the elements for the single-element materials, binary compounds, and both single-element materials and binary compounds, respectively.

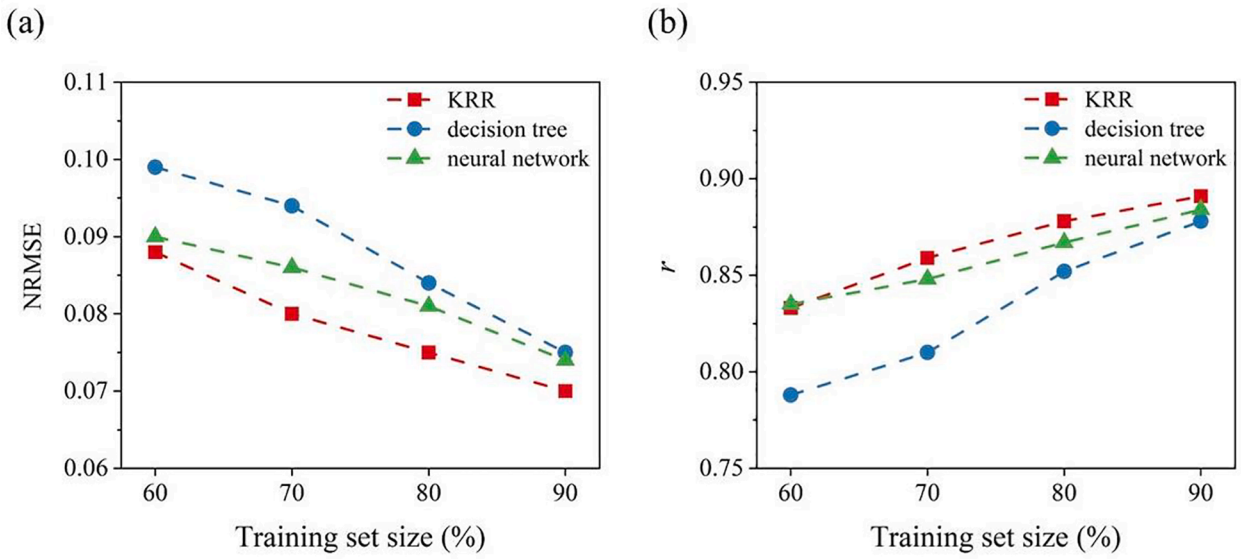

Fig. 3. NRMSE and *r* for KRR, decision tree, and neural network. The training sets are set as 60%, 70%, 80%, and 90% of the dataset for training.

large feature importance. For intrinsic features of materials, the mass density and mean atomic mass are related to the sizes of nuclei and the interspace between the nuclei. If the interspace is larger than the distance of defects' migration, the defects could be absorbed or annihilated, otherwise the defect generating process should dominate [56]. On the other hand, Poisson's ratio is one of the important mechanical properties for DGE, which is related to the interatomic bond angle and bond energy. Previous studies on dislocation dynamics have found that small Poisson's ratio would increase the strain energy per unit length of edge dislocation [57–59], namely, amorphization is related to Poisson's ratio [60]. The atomic mass difference implies the imbalance of atoms' responses to radiation due to different atomic masses between the heavy and light atoms. During the ballistic cascade, the light atoms vibrate rapidly to induce defects and transfer energy [61], which is supposed to be the key point. Furthermore, the importance of atomic mass difference inspires us to control the DGE by light atom doping. For instance, it was reported that potassium doped tungsten shows higher radiation tolerance than pure tungsten [62], because potassium doping optimizes the grain size of the crystal and defects could diffuse to the grain boundaries in shorter paths. Thus, it further demonstrates that the light atoms can control the DGE by altering the grain sizes of a material. The reasonable feature importance shows the correctness of our ML models.

In Fig. 4(a), it is obvious that some of the features only make negligible contributions to the model. Thus, to simplify the model, we compress the dataset by omitting these features. For comparison, the principal component analysis (PCA) is also implemented. The percentages of variances contributed by principal components are given in Fig. 4(b), showing that the sum of five largest components is 70.2%, which is similar to the feature importance provided by the decision tree. Both of PCA's results and that of the decision tree show the validation of dataset compression. Therefore, we build a new dataset with the five important features combined with the direction of PKA's velocity,

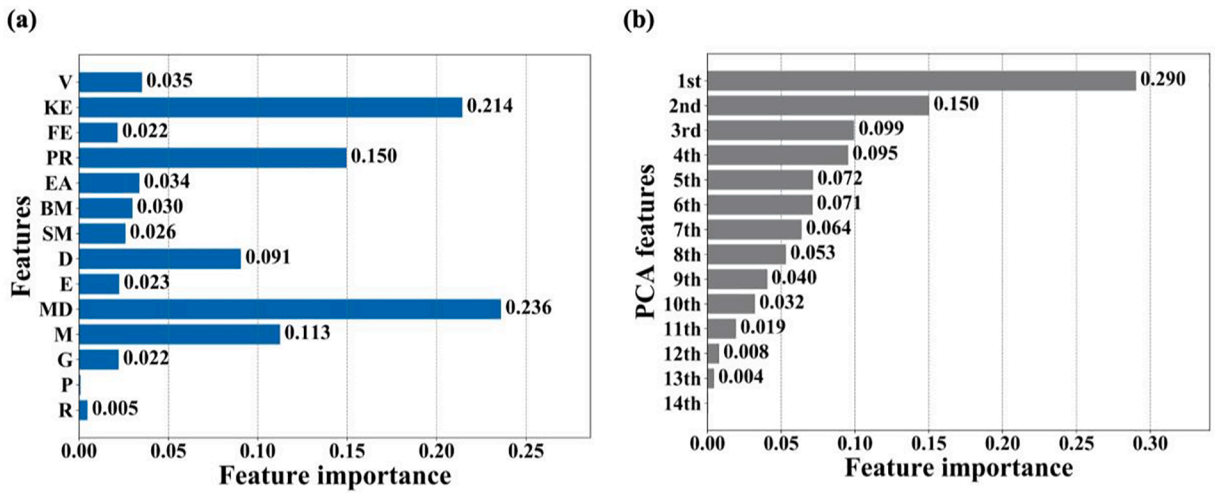

Fig. 4. (a) Feature importance plot for the mean atomic radius (R), mean period (P), mean group (G), mean atomic mass (M), atomic mass difference (MD), number of valence electrons (E), mass density (D), shear modulus (SM), bulk modulus (BM), elastic anisotropy (EA), Poisson's ratio (PR), formation energy (FE), kinetic energy of PKA (KE), direction of PKA's velocity (V). (b) Contributions to the variances of the features by fourteen principal components in PCA.

named dataset-6.

3.3. Predicting new materials with low defect generation efficiency

The prediction of new low DGE materials can be achieved with the well-trained ML models by three steps: (1) Fix the parameters of ML models; (2). Treat the ML model as a function and the input features as new variables; (3). Utilize optimization methods to find local minimum points with respect to the input features. As a result, the minimum points correspond to possible low DGE materials. We can find the desired materials by comparing the features of the materials with our predicted features, and the matched one is the desirable low DGE material. However, in our models, the decision tree should be excluded first, since the derivative of decision-tree function is either zero or infinity with respect to features [29], which cannot be optimized using gradient-descent based methods [63]. On the other hand, the minimum points from the model may have no correspondence in real materials due to the large feature distance illustrated above. In order to improve the efficiency, we use the dataset-6 to reduce the interference of unimportant features without a significant loss of accuracy. The performances of KRR and neural network on the new dataset are shown in Fig. 5(a). Only the neural network gives acceptable results. Therefore, the neural network is used for seeking new low DGE materials. Moreover, the cross-validation results of the neural network are plotted in Fig. 5 (b), which shows that the majority is on the line, in good agreement with the results in Fig. 5(a).

We train the neural network on the whole new dataset and make some predictions. One of the predicted possible low DGE materials, Zr_6Ni_{23} is listed in Table. 1 (the Poisson's ratio is omitted due to the lack of data). To further confirm the rationality, the defect ratio of Zr_6Ni_{23} is calculated by using a supercell of $15 \times 15 \times 15$ for keeping the similar

Table 1
Comparison of the predicted features using well-trained neural network (predicted) with the (calculated) features of mean atomic mass (M), atomic mass difference (MD), and mass density (D) for Zr_6Ni_{23}.

	M (amu)	MD (amu)	D (g/cm^3)
predicted	66.88	34.95	8.59
calculated	65.43	32.52	8.45

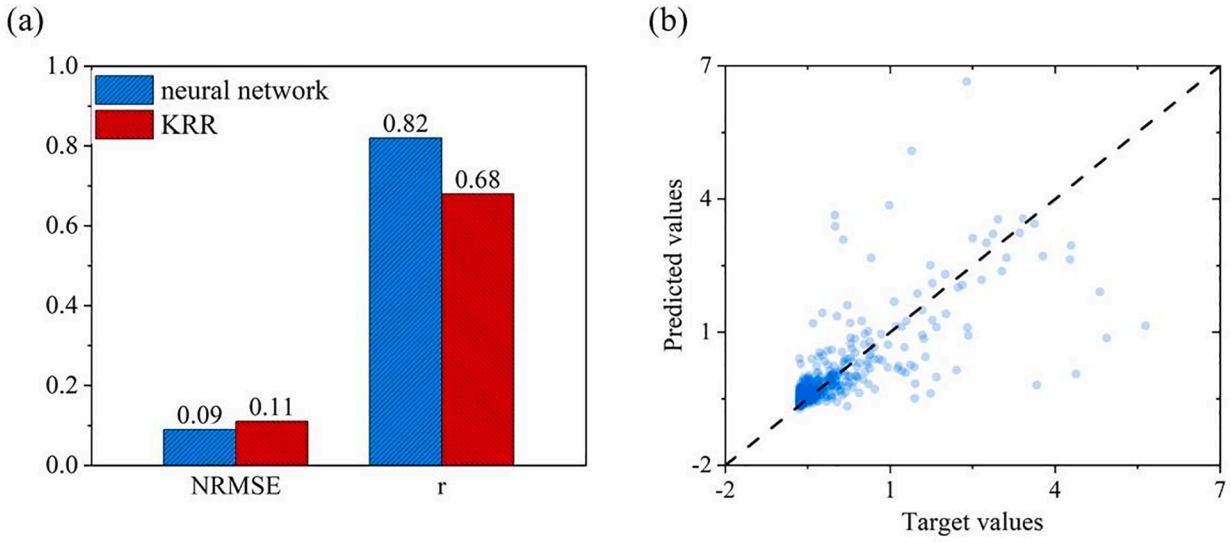

Fig. 5. (a) Performance of neural network and KRR trained with dataset-6, the training set is randomly set to 90% of the dataset. The results are the average of 100 trials. (b) Learning performance between the predicted values of the neural network and standardized targets of the dataset.

cell size and the number of atoms as our dataset. The defect ratio of Zr_6Ni_{23} is 3.24E-3, while the average defect ratio of the dataset is 6.00E-3, which confirms our prediction that Zr_6Ni_{23} is a material with low defect generation efficiency. With the development of computational materials science, more low DGE materials will be reported, which can be used to build more complete dataset, then the accuracy of the prediction would be improved.

4. Conclusions

In summary, based on the results of molecular dynamics simulations, we have constructed a dataset containing 444 samples including single-element materials and binary compounds. By using three ML models, i.e. decision tree, KRR, and neural network, to train the dataset, we have identified four important intrinsic features of materials, namely, atomic mass difference, Poisson's ratio, mean atomic mass, and mass density, which have a crucial effect on the DGE of materials. Furthermore, a new dataset is constructed by using these features combined with two environmental features, named dataset-6. Next, the KRR and neural network models are trained with the dataset-6 to predict new low DGE materials. Finally, Zr_6Ni_{23} as one of our predictions is confirmed to be a low DGE material by molecular dynamics method, demonstrating the validity and high efficiency of our models. The method of using the optimization method with respect to the input features for predicting new low DGE materials would be helpful in screening radiation-tolerant materials.

CRediT authorship contribution statement

Dongyuan Ni: Conceptualization, Methodology, Software, Writing - original draft, Writing - review & editing. **Wei Wu:** Writing - review & editing. **Yaguang Guo:** Writing - review & editing. **Sheng Gong:** Writing - review & editing. **Qian Wang:** Writing - review & editing, Supervision.

Declaration of Competing Interest

The authors declare that they have no known competing financial interests or personal relationships that could have appeared to influence the work reported in this paper.

Acknowledgements

This work is partially supported by grants from the National Science Foundation China (Grants No. NSFC-21773004 and NSFC-11974028), and the National Key Research and Development Program of the Ministry of Science and Technology of China (2017YFA0205003), and is supported by the High-Performance Computing Platform of Peking University, China.

Appendix A. Supplementary data

Supplementary data to this article can be found online at https://doi.org/10.1016/j.commatsci.2021.110306.

References

[1] R. Sharp, M. Decréton, Radiation tolerance of components and materials in nuclear robot applications, Reliab. Eng. Syst. Saf. 53 (3) (1996) 291–299.
[2] S.J. Zinkle, L.L. Snead, Designing Radiation Resistance in Materials for Fusion Energy, Annu. Rev. Mater. Res. 44 (1) (2014) 241–267.
[3] .U. Youk, N.H. Lee, B.S. Kim, Y.B. Lee, K. Seungho, Technology development for the radiation hardening of robots. In: Proceedings 1999 IEEE/RSJ International Conference on Intelligent Robots and Systems. Human and Environment Friendly Robots with High Intelligence and Emotional Quotients (Cat. No.99CH36289), vol. 3, 1999, pp. 1715–1720.
[4] K. Jin, H. Bei, Y. Zhang, Ion irradiation induced defect evolution in Ni and Ni-based FCC equiatomic binary alloys, J. Nucl. Mater. 471 (2016) 193–199.
[5] J.S. Zhen, Q. Yang, Y.H. Yan, X.W. Jiang, S.A. Yan, W. Chen, X.Q. Guo, Molecular dynamics study of structural damage in amorphous silica induced by swift heavy-ion radiation, Radiat Eff. Defects Solids 171 (3–4) (2016) 340–349.
[6] K.P. Zolnikov, A.V. Korchuganov, D.S. Kryzhevich, V.M. Chernov, S.G. Psakhie, Structural changes in elastically stressed crystallites under irradiation, Nucl. Instrum. Methods Phys. Res., Sect. B 352 (2015) 43–46.
[7] A.V. Korchuganov, K.P. Zolnikov, D.S. Kryzhevich, Simulation of interaction of edge dislocations with radiation defects in Fe-10Cr alloy, J. Phys. Conf. Ser. 1115 (2018), 052032.
[8] K.E. Sickafus, L. Minervini, R.W. Grimes, J.A. Valdez, M. Ishimaru, F. Li, K. J. McClellan, T. Hartmann, Radiation tolerance of complex oxides, Science 289 (5480) (2000) 748.
[9] W. Zhang, P.K. Liaw, Y. Zhang, Science and technology in high-entropy alloys, Sci. China Mater. 61 (1) (2018) 2–22.
[10] T. Yang, S. Xia, S. Liu, C. Wang, S. Liu, Y. Fang, Y. Zhang, J. Xue, S. Yan, Y. Wang, Precipitation behavior of AlxCoCrFeNi high entropy alloys under ion irradiation, Sci. Rep. 6 (2016) 32146.
[11] O. El-Atwani, N. Li, M. Li, A. Devaraj, J.K.S. Baldwin, M.M. Schneider, D. Sobieraj, J.S. Wróbel, D. Nguyen-Manh, S.A. Maloy, E. Martinez, Outstanding radiation resistance of tungsten-based high-entropy alloys, Sci. Adv. 5 (3) (2019) eaav2002.
[12] K. Trachenko, J.M. Pruneda, E. Artacho, M.T. Dove, How the nature of the chemical bond governs resistance to amorphization by radiation damage, Phys. Rev. B 71 (18) (2005), 184104.
[13] K. Trachenko, M.T. Dove, E. Artacho, I.T. Todorov, W. Smith, Atomistic simulations of resistance to amorphization by radiation damage, Phys. Rev. B 73 (17) (2006), 174207.
[14] X. Wang, Y.-T. Zhang, P.-C. Liu, J. Yan, W. Mo, P.-C. Zhang, X.-Q. Chen, Ductile-to-brittle transition and materials' resistance to amorphization by irradiation damage, RSC Adv. 6 (50) (2016) 44561–44568.
[15] K. Imada, M. Ishimaru, H. Xue, Y. Zhang, S.C. Shannon, W.J. Weber, Amorphization resistance of nano-engineered SiC under heavy ion irradiation, J. Nucl. Mater. 478 (2016) 310–314.
[16] A. Meldrum, L.A. Boatner, R.C. Ewing, Displacive radiation effects in the monazite- and zircon-structure orthophosphates, Phys. Rev. B 56 (21) (1997) 13805–13814.
[17] N. Swaminathan, M. Wojdyr, D.D. Morgan, I. Szlufarska, Radiation interaction with tilt grain boundaries in β-SiC, J. Appl. Phys. 111 (5) (2012), 054918.
[18] K.E. Sickafus, R.W. Grimes, J.A. Valdez, A. Cleave, M. Tang, M. Ishimaru, S. M. Corish, C.R. Stanek, B.P. Uberuaga, Radiation-induced amorphization resistance and radiation tolerance in structurally related oxides, Nat. Mater. 6 (3) (2007) 217–223.
[19] F. Garrido, S. Moll, G. Sattonnay, L. Thomé, L. Vincent, Radiation tolerance of fluorite-structured oxides subjected to swift heavy ion irradiation, Nucl. Instrum. Methods Phys. Res., Sect. B 267 (8) (2009) 1451–1455.
[20] K.E. Sickafus, J.A. Valdez, J.R. Williams, R.W. Grimes, H.T. Hawkins, Radiation induced amorphization resistance in A2O3–BO2 oxides, Nucl. Instrum. Methods Phys. Res., Sect. B 191 (1) (2002) 549–558.
[21] A. Meldrum, L.A. Boatner, R.C. Ewing, Effects of ionizing and displacive irradiation on several perovskite-structure oxides, Nucl. Instrum. Methods Phys. Res., Sect. B 141 (1) (1998) 347–352.
[22] K.T. Butler, D.W. Davies, H. Cartwright, O. Isayev, A. Walsh, Machine learning for molecular and materials science, Nature 559 (7715) (2018) 547–555.
[23] M. Gastegger, L. Schwiedrzik, M. Bittermann, F. Berzsenyi, P. Marquetand, wACSF—Weighted atom-centered symmetry functions as descriptors in machine learning potentials, J. Chem. Phys. 148 (24) (2018), 241709.
[24] T. Xie, J.C. Grossman, Crystal graph convolutional neural networks for an accurate and interpretable prediction of material properties, Phys. Rev. Lett. 120 (14) (2018), 145301.
[25] G. Pilania, K.R. Whittle, C. Jiang, R.W. Grimes, C.R. Stanek, K.E. Sickafus, B. P. Uberuaga, Using machine learning to identify factors that govern amorphization of irradiated pyrochlores, Chem. Mater. 29 (6) (2017) 2574–2583.
[26] K. Nordlund, S.J. Zinkle, A.E. Sand, F. Granberg, R.S. Averback, R.E. Stoller, T. Suzudo, L. Malerba, F. Banhart, W.J. Weber, F. Willaime, S.L. Dudarev, D. Simeone, Primary radiation damage: A review of current understanding and models, J. Nucl. Mater. 512 (2018) 450–479.
[27] S.I. Samarin, V.V. Dremov, A hybrid model of primary radiation damage in crystals, J. Nucl. Mater. 385 (1) (2009) 83–87.
[28] G. Pilania, C. Wang, X. Jiang, S. Rajasekaran, R. Ramprasad, Accelerating materials property predictions using machine learning, Sci. Rep. 3 (1) (2013) 2810.
[29] R. Fernandez Martinez, A. Okariz, J. Ibarretxe, M. Iturrondobeitia, T. Guraya, Use of decision tree models based on evolutionary algorithms for the morphological classification of reinforcing nano-particle aggregates, Comput. Mater. Sci. 92 (2014) 102–113.
[30] A. Gajewicz, T. Puzyn, K. Odziomek, P. Urbaszek, A. Haase, C. Riebeling, A. Luch, M.A. Irfan, R. Landsiedel, M. van der Zande, H. Bouwmeester, Decision tree models to classify nanomaterials according to the DF4nanoGrouping scheme, Nanotoxicology 12 (1) (2018) 1–17.
[31] F. Baras, O. Politano, Molecular dynamics simulations of nanometric metallic multilayers: Reactivity of the Ni-Al system, Phys. Rev. B 84 (2) (2011), 024113.
[32] J.R. Perilla, B.C. Goh, C.K. Cassidy, B. Liu, R.C. Bernardi, T. Rudack, H. Yu, Z. Wu, K. Schulten, Molecular dynamics simulations of large macromolecular complexes, Curr. Opin. Struct. Biol. 31 (2015) 64–74.
[33] S. Chmiela, H.E. Sauceda, K.-R. Müller, A. Tkatchenko, Towards exact molecular dynamics simulations with machine-learned force fields, Nat. Commun. 9 (1) (2018) 3887.
[34] A. Jain, S.P. Ong, G. Hautier, W. Chen, W.D. Richards, S. Dacek, S. Cholia, D. Gunter, D. Skinner, G. Ceder, K.A. Persson, Commentary: The Materials Project:

a materials genome approach to accelerating materials innovation, APL Mater. 1 (1) (2013), 011002.
[35] S. Plimpton, Fast parallel algorithms for short-range molecular dynamics, J. Comput. Phys. 117 (1) (1995) 1–19.
[36] C.A. Becker, F. Tavazza, Z.T. Trautt, R.A. Buarque de Macedo, Considerations for choosing and using force fields and interatomic potentials in materials science and engineering, Curr. Opin. Solid State Mater. Sci. 17 (6) (2013) 277–283.
[37] Y. Mishin, A.Y. Lozovoi, Angular-dependent interatomic potential for tantalum, Acta Mater. 54 (19) (2006) 5013–5026.
[38] J. Tersoff, New empirical model for the structural properties of silicon, Phys. Rev. Lett. 56 (6) (1986) 632–635.
[39] J. Tersoff, New empirical approach for the structure and energy of covalent systems, Phys. Rev. B 37 (12) (1988) 6991–7000.
[40] S. Miyashiro, S. Fujita, T. Okita, H. Okuda, MD simulations to evaluate effects of applied tensile strain on irradiation-induced defect production at various PKA energies, Fusion Eng. Des. 87 (7) (2012) 1352–1355.
[41] A.J.E. Foreman, C.A. English, W.J. Phythian, Molecular dynamics calculations of displacement threshold energies and replacement collision sequences in copper using a many-body potential, Philos. Mag. A 66 (5) (1992) 655–669.
[42] H. Huang, X. Tang, F. Chen, Y. Yang, J. Liu, H. Li, D. Chen, Radiation damage resistance and interface stability of copper–graphene nanolayered composite, J. Nucl. Mater. 460 (2015) 16–22.
[43] A. Stukowski, Visualization and analysis of atomistic simulation data with OVITO–the Open Visualization Tool, Modell. Simul. Mater. Sci. Eng. 18 (1) (2009), 015012.
[44] F. Pedregosa, Ga, #235, l. Varoquaux, A. Gramfort, V. Michel, B. Thirion, O. Grisel, M. Blondel, P. Prettenhofer, R. Weiss, V. Dubourg, J. Vanderplas, A. Passos, D. Cournapeau, M. Brucher, M. Perrot, #201, d. Duchesnay, Scikit-learn: Machine Learning in Python, J. Mach. Learn. Res. 12 (2011) 2825–2830.
[45] A. Paszke, S. Gross, S. Chintala, G. Chanan, E. Yang, Z. DeVito, Z. Lin, A. Desmaison, L. Antiga, A. Lerer, Automatic differentiation in pytorch, (2017).
[46] X.-X. Su, Y.-F. Wang, Y.-S. Wang, Effects of Poisson's ratio on the band gaps and defect states in two-dimensional vacuum/solid porous phononic crystals, Ultrasonics 52 (2) (2012) 255–265.
[47] F. Scarpa, S. Adhikari, C.Y. Wang, Mechanical properties of non-reconstructed defective single-wall carbon nanotubes, J. Phys. D Appl. Phys. 42 (14) (2009), 142002.
[48] M.L. Dunn, H. Ledbetter, Poisson's ratio of porous and microcracked solids: Theory and application to oxide superconductors, J. Mater. Res. 10 (11) (1995) 2715–2722.
[49] L.K. Mansur, Irradiation creep by climb-enabled glide of dislocations resulting from preferred absorption of point defects, Philos. Mag. A 39 (4) (1979) 497–506.
[50] L. Yuan, Q. Sun, B. Lehman, S. Lu, H.F. Hamann, J. Simmons, J. Black, A machine-learning approach for regional photovoltaic power forecasting, in: 2016 IEEE Power and Energy Society General Meeting (PESGM), 2016, pp. 1–5.
[51] X. Jiang, H.-Q. Yin, C. Zhang, R.-J. Zhang, K.-Q. Zhang, Z.-H. Deng, G.-Q. Liu, X.-H. Qu, An materials informatics approach to Ni-based single crystal superalloys lattice misfit prediction, Comput. Mater. Sci. 143 (2018) 295–300.
[52] Y. Zhang, C. Ling, A strategy to apply machine learning to small datasets in materials science, npj Comput. Mater. 4 (1) (2018) 25.
[53] A.o. Furmanchuk, J.E. Saal, J.W. Doak, G.B. Olson, A. Choudhary, A. Agrawal, Prediction of seebeck coefficient for compounds without restriction to fixed stoichiometry: A machine learning approach, J. Comput. Chem. 39(4) (2018) 191–202.
[54] A. Mangal, E.A. Holm, A comparative study of feature selection methods for stress hotspot classification in materials, Integr. Mater. Manuf. Innov. 7 (3) (2018) 87–95.
[55] M.T. Robinson, O.S. Oen, The channeling of energetic atoms in crystal lattices, Appl. Phys. Lett. 2 (2) (1963) 30–32.
[56] E.M. Bringa, J.D. Monk, A. Caro, A. Misra, L. Zepeda-Ruiz, M. Duchaineau, F. Abraham, M. Nastasi, S.T. Picraux, Y.Q. Wang, D. Farkas, Are nanoporous materials radiation resistant? Nano Lett. 12 (7) (2012) 3351–3355.
[57] J. Weiss, F. Lahaie, J.R. Grasso, Statistical analysis of dislocation dynamics during viscoplastic deformation from acoustic emission, J. Geophys. Res. Solid Earth 105 (B1) (2000) 433–442.
[58] R. Maaß, M. Wraith, J.T. Uhl, J.R. Greer, K.A. Dahmen, Slip statistics of dislocation avalanches under different loading modes, Phys. Rev. E 91 (4) (2015), 042403.
[59] H. Song, D. Dimiduk, S. Papanikolaou, Universality class of nanocrystal plasticity: localization and self-organization in discrete dislocation dynamics, Phys. Rev. Lett. 122 (17) (2019), 178001.
[60] J.R. Xiao, J. Staniszewski, J.W. Gillespie, Tensile behaviors of graphene sheets and carbon nanotubes with multiple Stone-Wales defects, Mater. Sci. Eng., A 527 (3) (2010) 715–723.
[61] F. Banhart, Irradiation effects in carbon nanostructures, Rep. Prog. Phys. 62 (8) (1999) 1181–1221.
[62] X. Shu, B. Huang, D. Liu, H. Fan, N. Liu, J. Tang, Effects of low energy helium plasma irradiation on potassium doped tungsten, Fusion Eng. Des. 117 (2017) 8–13.
[63] D.E. Rumelhart, G.E. Hinton, R.J. Williams, Learning representations by back-propagating errors, Nature 323 (6088) (1986) 533–536.